International Journal of Refractory Metals and Hard Materials 118 (2024) 106480

Contents lists available at ScienceDirect

International Journal of Refractory Metals and Hard Materials

journal homepage: www.elsevier.com/locate/IJRMHM

Prediction of hardmetal corrosion based on the binder response

A.M. Ferro Rocha [a], A.M. Santos [a], R. Mineiro [a], P. Pereira [b], J. Sacramento [b,c], A.M.R. Senos [a], A.C. Bastos [a,*]

[a] Department of Materials and Ceramic Engineering, CICECO – Aveiro Institute of Materials, University of Aveiro, 3810-193 Aveiro, Portugal
[b] DURIT – Metalurgia Portuguesa do Tungsténio, Lda, 3854-909 Albergaria-a-Velha, Portugal
[c] ESTGA – Águeda School of Technology and Management, University of Aveiro, 3754-909 Águeda, Portugal

ARTICLE INFO

Keywords:
Hardmetals
Alternative binders
Corrosion behaviour
Galvanic corrosion
Electrochemistry

ABSTRACT

For 100 years WC-Co has been the quintessential hardmetal, finding extensive application whenever high hardness and wear resistance are required. However, recent concerns regarding health and economic factors have motivated both industry and academia to explore alternative composites. Consequently, numerous hard phases and metallic binders are currently under evaluation. To expedite and streamline the development process, a crucial question arises: "Can the corrosion resistance of hardmetals be predicted based on the electrochemical behavior of their binders?". To help answer this question, this work compares the corrosion resistances of various hardmetal composites (WC-Co, WC-Ni, WC-CoNi, WC-CoCr, WC-NiCr, WC-CoNiCr, WC-NiCrMo, and WC-FeCoNi) to the corrosion resistances of binder analogues (Co, Ni, CoNi, CoCr, NiCr, CoNiCr, NiCrMo, and FeCoNi) in a 0.5 M NaCl solution using electrochemical techniques: open circuit potential monitoring, polarisation curves and galvanic current between WC and binder measured with zero resistance ammeter (ZRA).

1. Introduction

For the past 100 years, hardmetals have been widely utilised in applications that demand high hardness and wear resistance, including cutting, drilling, drawing, extrusion, aerospace coatings, and valves and seals for pumping systems [1–3]. Among hardmetals, WC-Co stands as the architype. It comprises micrometer-sized particles of hard but brittle tungsten monocarbide (WC) bound together by a ductile cobalt (Co) phase. The exceptional wetting properties of Co towards WC enable the production of dense, homogeneous sintered materials with high hardness and good fracture thoughness [1–3]. These properties placed WC-Co as the leading hardmetal for the past century. However, concerns have arisen regarding the health implications associated with both WC and Co [4–6]. Additionally, the inclusion of tungsten (W) and cobalt in Eurpope's list of critical raw materials [7] prompted the industry and academia to explore alternative composites [8–10]. Furthermore, the corrosion resistance of WC-Co often proves inadequate [10–15], particularly in acidic environments [16–21]. Consequently, many alloys are being tested as binders in a trial-and-error basis. The development process can be expedited if the corrosion resistance of hardmetals could be predicted based on the electrochemical response of the binder.

To test this hypothesis, this work compares the electrochemical response of several hardmetal composites (WC-Co, WC-Ni, WC-CoNi, WC-CoCr, WC-NiCr, WC-CoNiCr, WC-NiCrMo, and WC-FeCoNi) with that of binder analogues (Co, Ni, CoNi, CoCr, NiCr, CoNiCr, NiCrMo, and FeCoNi) manufactured by the same powder metallurgy methods and composition based on the composites starting raw materials. The electrochemical investigation was carried out in aerated aqueous solution of 0.5 M NaCl using various electrochemical techniques, including open circuit potential monitoring (OCP), potentiodynamic polarisation curves, and galvanic current measurement between the WC hard phase and the binders utilising a zero resistance ammeter (ZRA).

The corrosion of hardmetals is usually considered to be dominated by the galvanic coupling of the metallic binder which oxidizes preferently and is accelerated by the additional cathodic activity occuring at the surface of the WC particles [20,22]. Hihara and Latanision, in their review of metal matrix composites corrosion [23] demonstrated how corrosion in such composites can be predicted by utilising polarisation data and the mixed potential theory [24,25]. The intersection of the cathodic curve of the nobler hard phase and the anodic curve of the metallic binder identifies the galvanic current of the couple. Depending on the environment and the electrochemical responses of the anode and cathode, various scenarios can appear. Typically, the corrosion current of the active metal will increase from its normal corrosion current (i_{corr})

---

* Corresponding author.
E-mail address: acbastos@ua.pt (A.C. Bastos).

https://doi.org/10.1016/j.ijrmhm.2023.106480
Received 2 July 2023; Received in revised form 26 October 2023; Accepted 30 October 2023

to the galvanic current (i_{Galv}) when coupled with the conductive hard material (cathode). However, if the binder is an active-passive metal, galvanic coupling in aerated conditions can polarise the metal into the passive region, providing anodic protection. In this case $i_{Galv} < i_{corr}$. For a passive metal i_{corr} and i_{Galv} will be identical in a halide-free environment, but in a halide-containing environment, pitting may occur in the galvanic couple, even though it will not happen when the metal is uncoupled. The corrosion behaviour may differ from that predicted using the mixed potential theory. Discrepancies can be identified by comparing the experimental polarisation diagram of the composite with that of the mixed electrode model generated from the data of the individual constituents. Such discrepancies often arise from processing effects, like segregation of alloying elements, formation of new phases, or introduction of impurities.

2. Experimental procedure

2.1. Materials and processing

The raw materials were WC powder (grain size = 0.8 μm, except ~1.5 μm for WC-FeCoNi), Cr_3C_2 and FeCoNi from H.C. Starck GmbH (Germany), Co from Umicore (Belgium), Ni from A.M.P.E.R.E. Industrie SASU (France) and Mo_2C from Treibacher Industrie AG (Austria). The eight hardmetal composites were prepared by conventional powder metallurgy methods. The powder mixtures were mixed in a roller ball mill, using ethanol and 5 mm hardmetal balls as grinding medium. The suspensions were dried and stored under vacuum until further use. Cylindrical green samples with 25 mm diameter and 10 mm thickness were die-pressed at 150 MPa. The samples were sintered in a sinter-HIP industrial furnace, at a maximum temperature of 1450 °C, under 30 bar of an argon atmosphere.

The amounts of the starting raw materials for each hardmetal composite are presented in Table 1. Also presented is the total carbon content of the sintered composites as determined by a LECO C744 analyser. The relative areas of WC and binder phases were determined by digital analysis of scanning electron microscopy images of the composites surfaces and are presented in Table 1. Binder analogues were manufactured by the same powder metallurgy methods. Their compositions were based on the starting materials of the corresponding composites and are presented in Table 2. The actual compositions of the binders in the composites were estimated by thermodynamic calculations, based on the CALPHAD methodology, carried out using the Thermo-Calc software (version 2023a with the commercial TCFE11 Steels/Fe-alloys database) to establish the phase equilibria for each system. The composition of the binder phase after sintering was assessed assuming the freezing of the microstructure at ~1000 °C during cooling from the maximum sintering temperature and considering the total carbon content of each sample determined experimentally. The values are presented in Table 2.

The porosity and microstructural features of the surface were observed on polished and etched samples by Light Optical Microscopy (Leica DM2500) and Scanning Electron Microscopy (Hitachi-SU-70) in accordance with ISO 4499-4:2016. The density of the sintered samples was measured according to Archimedes' principle (ISO 3369:2006). Vickers hardness (ISO 6507-1:2018) was measured with a load of 30 kgf, and the fracture toughness (K_{IC}) was calculated from the Vickers indentation crack length using the Palmqvist method (ISO 28079:2009). More information regarding the fabrication of the composites and the characterization techniques for evaluating the microstructure, physical and mechanical properties can be found in [26].

2.2. Corrosion testing

For corrosion testing, samples of binders and composites were connected to copper wires with conductive silver paint (PELCO, USA), and mounted in epoxy resin (BUEHLER EpoKwick™ FC, USA). The surface was mirror polished before each experiment. The testing medium was aqueous 0.5 M NaCl solution prepared with distilled water and *pro analysis* grade reagent. For polarisation curves the tested area (0.24 cm^2 for all samples) was delimited with 3M™ Electroplating Tape 470. A standard three-electrode arrangement was used with a saturated calomel electrode (SCE) as reference, a platinum coiled wire as counter electrode and the exposed sample area as working electrode. The measurements were carried out using PGSTAT204 or PGSTAT302N potentiostats (Autolab, The Netherlands) with an electrochemical cell with 100 mL volume inside a Faraday cage, at room temperature (22 ± 2 °C) and open to air. The Open Circuit Potential (OCP) was monitored during the first hour of immersion. Then, potentiodynamic polarisation curves (anodic sweeps) were obtained from near −50 mV vs OCP to 1.2 V vs SCE, with a scan rate of 0.1 mV/s. The galvanic current and the potential

Table 1
Chemical composition of the composites.

Composites	Starting materials (wt%)						C in sintered material (%)	Area (%)	
	WC	Co	Ni	Fe	Cr_3C_2	Mo_2C		WC	Binder
WC-Co	92.0	8.0					5.6	87	13
WC-Ni	92.0		8.0				5.5	87	13
WC-CoNi	92.0	5.5	2.5				5.5	87	13
WC-CoCr	92.0	7.2			0.8		5.5	87	13
WC-NiCr	91.2		8.0		0.8		5.4	85	15
WC-CoNiCr	94.2	3.5	1.5		0.8		5.6	90	10
WC-NiCrMo	90.6		8.0		0.8	0.6	5.4	85	15
WC-FeCoNi	90	2.0	4.0	4.0			5.5	82	18

Table 2
Binders composition.

Composites	Manufactured binder (wt%)					Binder in composite (wt%)						
	Co	Ni	Cr	Mo	Fe	W	C	Co	Ni	Cr	Mo	Fe
WC-Co	100.0					5.5	0.1	94.4	–	–	–	–
WC-Ni		100.0				20.1	0.1	–	79.8	–	–	–
WC-CoNi	68.8	31.2				21.8	0.1	53.7	24.4	–	–	–
WC-CoCr	91.2		8.8			16.1	0.1	76.3	–	7.5	–	–
WC-NiCr		92.0	8.0			24.5	0.1	–	69.8	5.6	–	–
WC-CoNiCr	61.5	26.3	12.2			23.2	0.1	48.9	21.3	6.5	–	–
WC-NiCrMo		86.4	7.5	6.1		26.5	0.1	–	68.2	4.9	0.3	–
WC-FeCoNi	20	40			40	4.4	0.1	19.1	38.2	–	–	38.2

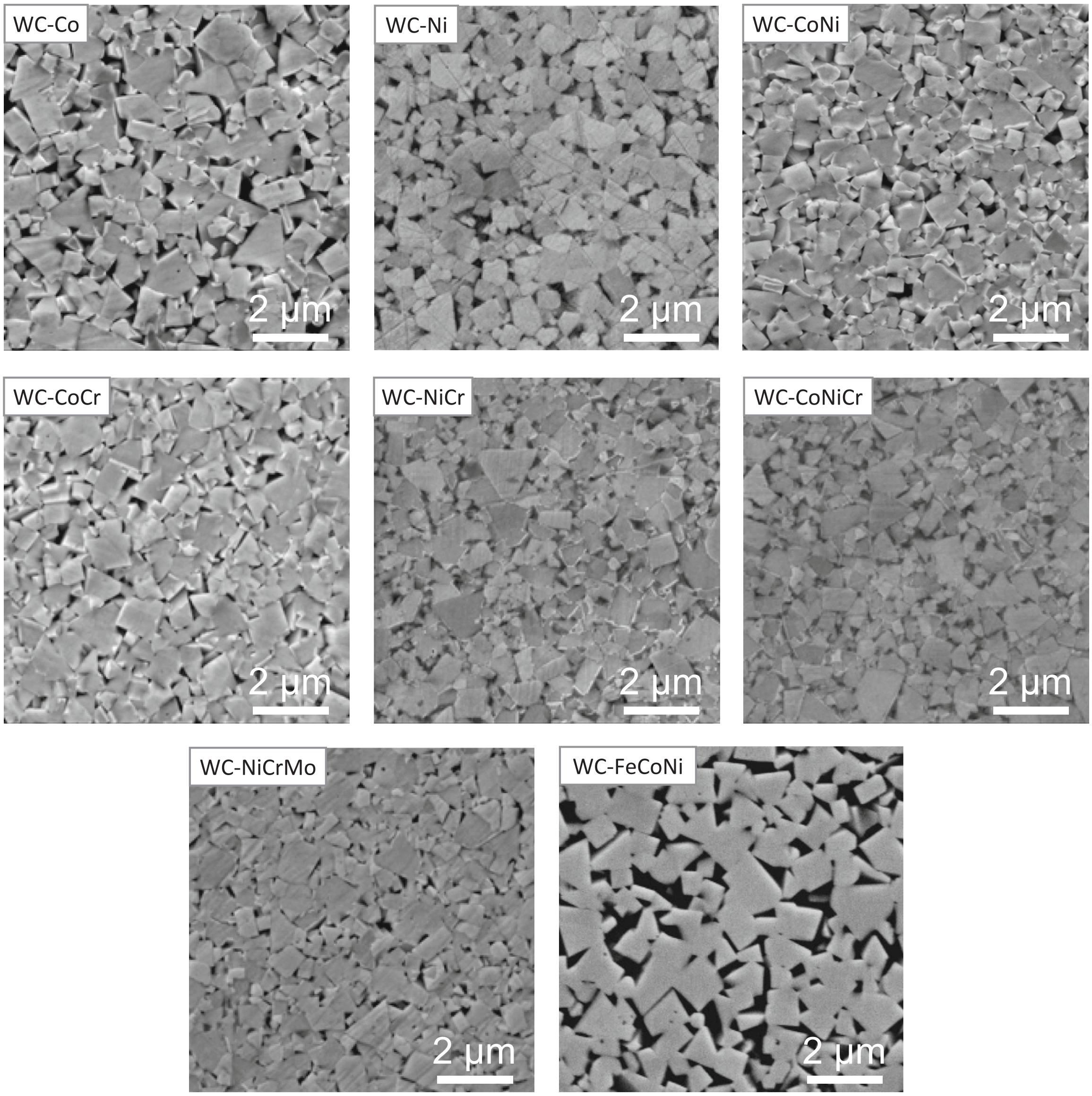

Fig. 1. SEM pictures of the composites' surfaces after etching in Murakami's solution (10 g potassium ferricyanide and 10 g sodium hydroxide in 100 mL distilled water).

of the coupling between binders and WC were measured with a Reference 600 potentiostat from Gamry Instruments (USA). The galvanic current was measured in ZRA (zero resistance ammeter) mode. The potential was measured vs SCE. In each experiment the WC and binder electrodes were placed one in front of the other at a distance of 1 cm. The areas of WC and binder were delimited so that their sum was 1 cm^2. The area ratio was that given in Table 1.

3. Results and discussion

3.1. Microstructure, physical and mechanical properties

Fig. 1 shows SEM (secondary electrons) micrographs of the composites. They are fully dense with no trace of porosity. The WC grains were well distributed in the binder matrix. Deleterious phases like free C or η-phase were not detected.

The physical and mechanical properties of the composites, the correlation with the microstructure and their tribological behaviour were studied before [26,27]. Table 3 summarises some of the most important parameters. WC-FeCoNi presented the lowest hardness and WC-CoNiCr the highest hardness. This should be related to the binder content, higher in the former and lower in the latter (Table 1). Note that the composites have a binder volume close to 13%, the notable exceptions being WC-FeCoNi with 18% and WC-CoNiCr with 10%. The fracture toughness of these composites lies within the acceptable range for hardmetals [28].

3.2. Corrosion testing

3.2.1. Open circuit potential

The corrosion potential of binder analogues and composites was measured during the first hour of immersion in 0.5 M NaCl. The results are presented in Fig. 2. For comparison, the potential of commercial pure metals obtained from Goodfellow (UK) or Mateck (Germany) are also presented. After variations in the first minutes of immersion most of the potentials were fairly stable by the end of the hour of measurement. It is worth mentioning that the potential of these composites was previously monitored for a period of 15 days [10] and, in some cases, the potentials continued evolving for a few days which means that the corrosion was still not in steady state. In general, a potential shift to

Table 3
Physical and mechanical properties of the composites [26,27].

Composite	Density[a] (g/cm^3)	Porosity[b]	G[c] (μm)	Hardness HV30 (kgf/mm^2)	K_{IC}^{d} (MPa. m$^{1/2}$)
WC-Co	14.72	A00B00C00	0.56	1659 ± 16	9.9 ± 0.13
WC-Ni	14.69	A00B00C00	0.57	1508 ± 16	9.4 ± 0.29
WC-CoNi	14.62	A00B00C00	0.55	1604 ± 22	9.5 ± 0.17
WC-CoCr	14.64	A00B00C00	0.57	1825 ± 6	9.3 ± 0.17
WC-NiCr	14.58	A00B00C00	0.54	1664 ± 8	9.5 ± 0.13
WC-CoNiCr	14.82	A00B00C00	0.54	1920 ± 18	8.8 ± 0.8
WC-NiCrMo	14.55	A00B00C00	0.53	1616 ± 11	9.0 ± 0.32
WC-FeCoNi	14.12	A00B00C00	0.81	1369 ± 12	10.5 ± 0.3

a Apparent density.
b ISO 4505:1978.
c Average of WC grain size.
d Palmqvist method.

more negative values is indicative of an increasing anodic area and corrosion activation of the surface whereas a positive shift is usually (but not necessarily) associated to the development of a surface protective layer. In Fig. 2 a) the pure metals showed potentials similar to those reported in the literature, with Fe being the most active with values close to −0.6 V vs SCE, while the other metals presented more positive values, between −0.2 and − 0.3 V vs SCE. The potential of the binder analogues is presented in Fig. 2 b) and the values spanned from close to −0.5 V of CoNiCr to near −0.2 V vs SCE of Ni. The additions of elements to Ni shifted the potential in the negative direction (more active potentials). The WC hard phase is electrically conductive and therefore it is electrochemically active [29,30]. Its potential is the most positive of all samples, being close to 0 V vs SCE. When WC and a metal are electrically connected like in a hardmetal composite, and immersed in an electrolyte solution, a galvanic couple is formed. Since WC has the most positive potential it will be the cathode of the galvanic couple while the metal binder will be the anode. The composites potential – presented in Fig. 2 c) – reflect this galvanic coupling. The potential of each composite is situated between the potential of WC and of the respective binder. The actual value depends on the oxidation rate of the anode. If the oxidation process is fast, then a slight positive polarisation of the binder (anode) is sufficient to match the increased cathodic current due to the galvanic coupling to WC (cathode). WC-Co, WC-FeCoNi and WC-CoCr are cases where the composite potential is just sligthly higher than the potential of the binder. Conversely, WC-NiCrMo and WC-CoNiCr presented shifts of 288 and 272 mV compared to the respective binder.

3.2.2. *Current-potential curves*

Fig. 3 shows the polarisation curves of commercially pure metals measured after 1 h of immersion in 0.5 M NaCl. The corrosion potentials, E_{corr}, were similar to those obtained in the OCP measurements being −0.574, −0.357, −0.220, −0.206 and − 0.267 V vs SCE for Fe, Co, Ni, Mo and Cr, respectively. The corrosion rates determined by Tafel

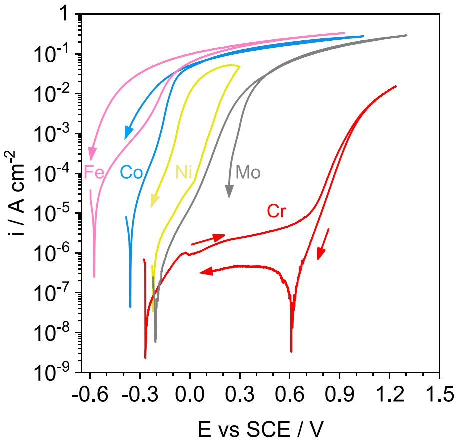

Fig. 3. Anodic polarisation curves of commercially pure (99.95 + %) Fe, Co, Ni, Mo, Cr after 1 h of immersion in 0.5 M NaCl.

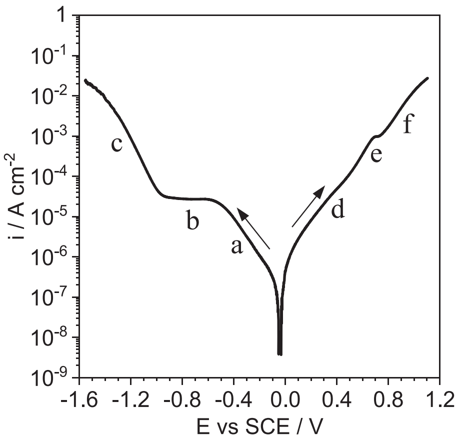

Fig. 4. Anodic and cathodic polarisation curves of WC measured after 1 h of immersion in 0.5 M NaCl.

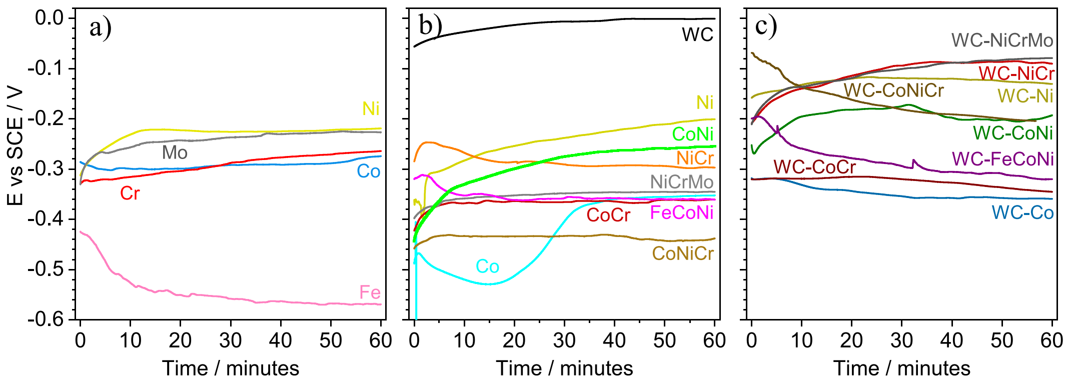

Fig. 2. Corrosion potential measured during the first hour of immersion in 0.5 M NaCl of a) commercially obtained pure metals, b) WC and binders produced by powder metallurgy, c) hardmetal composites.

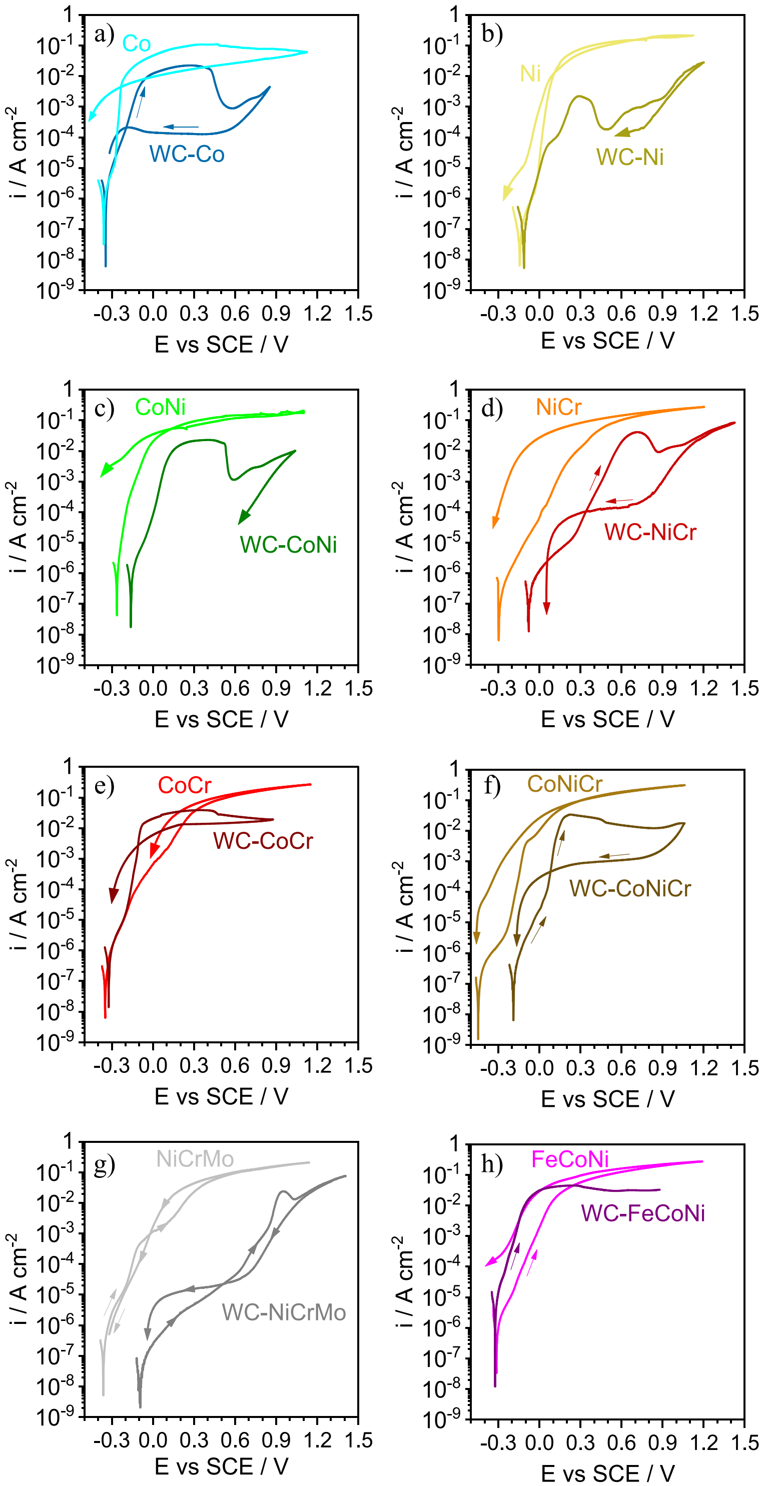

Fig. 5. Anodic polarisation curves of binders and composites acquired after 1 h of immersion in 0.5 M NaCl.f

extrapolation [25] were 55, 8.6, 1.4, 0.46 and 0.047 μA cm^{-2}, for Fe, Co, Ni, Mo and Cr, respectively. The metal oxidation can be described by the generic half-reaction,

$$M(s) \rightarrow M^{n+}(aq) + ne^{-} \quad (1)$$

where M = Fe, Co, Ni, Mo or Cr and $n = 2$ (Fe, Co, Ni), 3 (Cr) or 4 (Mo) [31].

Fe, Ni, Co and Mo depict an active behaviour with a noticeable increase in current as the potential sweeps in the positive direction. The high currents are maintained in the reverse scans and the return to zero occurs at potentials more negative than E_{corr}. Mo is the exception with the anodic current decreasing to zero around 0.235 V vs SCE. Cr shows a passive plateau until 0.75 V vs SCE when a transpassive dissolution takes place [32]. In the reverse scan the current is lower than in the forward scan which means that during the anodic polarisation the passive film strengthened.

Anodic and cathodic polarisation curves were obtained for the WC phase and the results are presented in Fig. 4. The different regions of the

Table 4
Electrochemical parameters (E_{corr}, i_{corr}, Tafel sloples) obtained from Figs. 2 and 5.

	Corrosion potential (mV_{SCE})		Current-potential curves					
	Binder	Composite	E_{corr} (mV_{SCE})		i_{corr} ($\mu A\ cm^{-2}$)		Tafel slope ($mV\ dec^{-1}$)	
			Binder	Composite	Binder	Composite*	Binder	Composite
WC-Co	−306 ± 35	−353 ± 7	−314 ± 26	−349 ± 8	16 ± 12	22 ± 2.6	73 ± 23	87 ± 3
WC-Ni	−229 ± 36	−130 ± 5	−230 ± 35	−99 ± 35	1.2 ± 0.9	2.2 ± 1.3	143 ± 22	146 ± 18
WC-CoNi	−225 ± 58	−188 ± 5	−215 ± 54	−164 ± 26	1.3 ± 0.8	11.0 ± 4.8	61 ± 13	159 ± 43
WC-CoCr	−355 ± 6	−331 ± 15	−355 ± 5	−307 ± 11	0.65 ± 0.19	18 ± 11	101 ± 0.5	112 ± 10
WC-NiCr	−294 ± 3	−95 ± 12	−296 ± 2	−67 ± 29	0.28 ± 0.01	2.7 ± 1.6	113 ± 14	238 ± 11
WC-CoNiCr	−462 ± 24	−190 ± 14	−472 ± 24	−182 ± 8	0.40 ± 0.13	12 ± 7.3	213 ± 36	120 ± 13
WC-NiCrMo	−367 ± 21	−79 ± 2	−355 ± 8	−87 ± 8	0.78 ± 0.04	1.0 ± 0.5	122 ± 0.7	190 ± 9
WC-FeCoNi	−336 ± 25	−320 ± 4	−336 ± 22	−297 ± 27	3.2 ± 1.8	27 ± 17	123 ± 6	53 ± 15

* Corrected for the binder area fraction (i_{corr} / area fraction of binder in the composite).

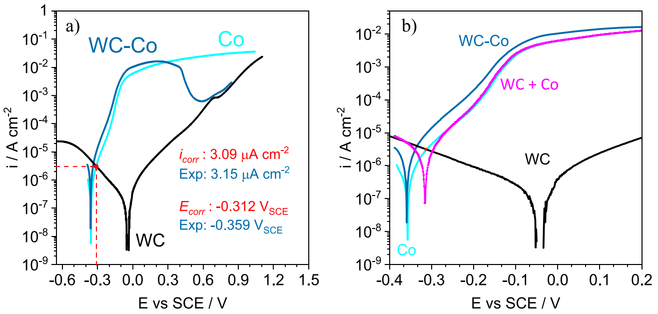

Fig. 6. a) Polarisation curves of WC-Co, and polarisation curves of Co and WC corrected for the respective areas in the composite; b) Reconstruction of the WC-Co polarisation curve from the curves of WC and Co.

curves are identified with letters from *a* to *f*. The segment *a* corresponds to the reduction of dissolved O_2 under activation control,

$$O_2(g) + 2H_2O(l) + 4e^- \rightarrow 4OH^-(aq) \tag{2}$$

In this region the current increases with the increase of the negative overpotential. At a certain point the transport of the reactant (O_2) to the surface reaches a limit and no further current increase is possible (unless the solution is stirred or O_2 is bubbled). A constant current is attained (limiting current of O_2 reduction), corresponding to segment *b*. At more negative overpotentials the reduction of water with production of hydrogen becomes possible and its current adds to the existing O_2 reduction current,

$$2H_2O(l) + 2e^- \rightarrow H_2(g) + 2OH^-(aq) \tag{3}$$

This corresponds to segment *c*. On the anodic side the current increases with the oxidation of WC [29,30,33] under activation control,

$$WC(s) + 5H_2O(l) \rightarrow WO_3(s) + CO_2(g) + 10H^+(aq) + 10e^- \tag{4}$$

This is a complex reaction with many electrons which means that a reaction mechanism lies behind. At 0.7 V vs SCE a quasi-passive plateau is observed (*e*) and credited to the effect of the WO_3 film over the WC in restricting the increment of the WC oxidation rate. In neutral and alkaline media WO_3 dissolves forming tungstate ion, WO_4^{2-} [30,34],

$$WO_3(s) + OH^-(aq) \rightarrow WO_4{}^{2-}(aq) + H^+(aq) \tag{5}$$

At high potentials WC can oxidize directly to tungstate [30,33,34],

$$WC(s) + 6H_2O(l) \rightarrow WO_4{}^{2-}(aq) + CO_2(g) + 12H^+(aq) + 10e^- \tag{6}$$

This reaction is responsible for segment *f*, in combination with the water oxidation [33],

$$2H_2O(l) \rightarrow O_2(g) + 4H^+(aq) + 4e^- \tag{7}$$

The polarisation curves of the composites and binders are presented in Fig. 5. The following analysis is based on existing literature. The reactions and films formed at the surface need experimental verification with spectroscopic methods, which was not performed in this work. Fig. 5 a) presents the electrochemical response of the Co binder analogue and the WC-Co composite, both prepared by powder metallurgy. The anodic current of Co exhibits a rapid increase until reaching a plateau. This plateau is observed in all polarisation curves of the binder analoguess in Fig. 5, and can be explained by the formation of a salt (chloride) or oxide layer in the presence of the local high concentration of metal ions generated at high current densities. This surface layer could deter the rise in the oxidation rate by acting as a diffusion barrier for the dissolved binder metal ions. It can also explain the lower currente measured in the reverse sweeps.

The curve of the WC-Co composite initially resembles that of the binder, but with a larger Tafel slope and a lower current density plateau. This difference is justified by the smaller surface area occupied by the

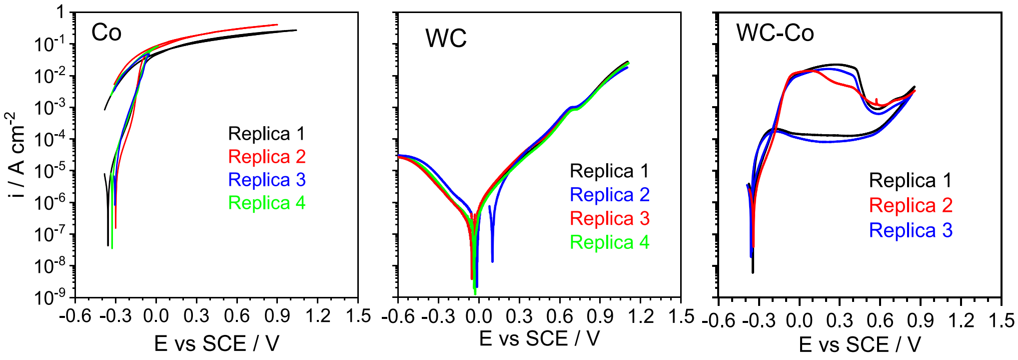

Fig. 7. Repeated polarisation curves of Co (binder), WC (hard phase) and WC-Co (composite) measured after 1 h of immersion in 0.5 M NaCl.

Table 5
E_{corr} and i_{corr} taken from the experimental polarisation curves, determined in the reconstructed curves (Fig. 6) and measured in the galvanic corrosion meausurements with a ZRA (Fig. 8).

	Anodic polarisation		Reconstruction		ZRA (1 h and *16 h*)	
	E_{corr} (V_{SCE})	i_{corr} ($\mu A\ cm^{-2}$)	E_{corr} (V_{SCE})	i_{corr} ($\mu A\ cm^{-2}$)	E_{couple} (V_{SCE})	I_{Galv} (μA)
WC-Co	−0.359	3.15	−0.312	3.09	−0.320 *(−0.450)*	17 *(5)*
WC-Ni	−0.135	0.46	−0.149	0.55	−0.020 *(−0.084)*	2.7 *(0.03)*
WC-CoNi	−0.166	1.23	−0.166	0.65	−0.211 *(−0.216)*	4 *(4)*
WC-CoCr	−0.298	1.30	−0.221	1.14	−0.270 *(−0.150)*	12.7 *(10)*
WC-NiCr	−0.078	0.69	−0.174	0.69	−0.148 *(−0.185)*	7 *(2.7)*
WC-CoNiCr	−0.190	0.44	−0.214	1.10	−0.303 *(−0.322)*	9.4 *(4.8)*
WC-NiCrMo	−0.094	0.09	−0.239	1.34	−0.172v *(−0.151)*	8 *(2)*
WC-FeCoNi	−0.324	7.83	−0.249	1.48	−0.154 *(−0.230)*	8 *(10)*

binder in the composite (accounting for only 13% of the total surface area). Interestingly, a notable decrease in current is observed at 0.4 V vs SCE. The plateau and the current decrease have been seen before and interpreted in terms of pseudopassivity [17,19,35]. This pseudopassivity has been explained in different ways. Human et al. [17] proposed the formation of an anodic film of $CoWO_4$ or $CuSO_4$ (in sulfuric acid environment) as the cause for the decrease in the measured current density. However, Sutthiruangwong et al. did not found such films and suggested two causes for the pseudopassivity [19,35]. The first was an increasing length for the diffusion path of cobalt ions through the porous WC skeleton which grows in depth as the Co dissolution progresses. The second was the presence of tungsten in the binder. W dissolves from WC during sintering yelding a Co—W alloy [17,19,35]. Tungsten in the binder improves the corrosion resistance of cemented carbides because tungsten oxides are formed on the surface of the binder decreasing its dissolution rate [19,35].

The formation of a Co—W alloy during the sintering of the composite was predicted by the thermodynamic calculations in Table 2 but the manufactured Co binder analogue does not contain W. In fact, all binders in the composites contain dissolved W some in significant amounts with impact in the corrosion resistance of the composite [19,35,36]. The binder analogues in this work were manufactured based on the starting raw materiais and do not contain W. This will be corrected in future studies.

After the pseudopassive region, for potentials higher than 0.6 V vs SCE, the current increases again due to reactions (6) and (7). In the return sweep, the current exhibits a plateau of significantly lower magnitude than in the forward sweep, as a manifestation of continuing pseudopassivity.

The polarisation curves of WC-CoNi, WC-CoCr and WC-CoNiCr present characteristics similar to the WC-Co curve but with different magnitudes due to the type and amount of alloying elements. The characteristics include a rapid increase in current, followed by current stabilization at high current densities, a subsequent decrease starting around 0.4 V vs SCE and finally, a reverse sweep with substantially lower current magnitudes. Chromium is known to act as an alloying element for the binder and for helping stabilising a cobalt-based oxide layer which inhibits dissolution of the binder [35].

The curves of the Ni-based binder analogues resemble the behaviour described for cobalt and commercially pure Ni. They display a rapid increase in current followed by a stabilization at high currents, with the reverse scan following the same path. The properties and corrosion behaviour of WC-Ni, WC-NiCr, and WC-NiCrMo hardmetals have been reviewed before [36]. A significant amount of dissolved W in the binder is always present. The addition of Cr and Mo to Ni significantly enhances the corrosion resistance of these alloys [36–38]. In Fig. 5, the Ni-based hardmetal composites show a current hump at progressively higher potentials: 0.3 V vs SCE for WC-Ni, 0.7 V vs SCE for WC-NiCr, and 0.95 V vs SCE for WC-NiCrMo. The passive current during the reverse scan was also progressively smaller: from 160 $\mu A\ cm^{-2}$ for WC-Ni, to 125 $\mu A\ cm^{-2}$ for WC-NiCr, and 18 $\mu A\ cm^{-2}$ for WC-NiCrMo, reflecting the impact of the alloying elements.

The last composite is WC-FeCoNi which showed a behaviour similar to the binder. Together with WC-Co it is the composite with lower corrosion resistance.

A general examination of the response of binders and composites in Fig. 5 reveals that, in most cases, the curves of the composites are shifted towards more noble potentials, with higher Tafel slopes, and a (pseudo) passive region in the reverse sweep.

The natural corrosion occurs at a single point of the polarisation curve, the corrosion potential, E_{corr}, with the corresponding corrosion current density, i_{corr}. These parameters were determined from 3-4 replicate measurements and are presented in Table 4. The open circuit potential (OCP) measured at the first hour of immersion (shown in Fig. 2) is also provided. The values obtained from OCP monitoring and polarisation curves show minimal differences. The composites consistently exhibited more positive corrosion potentials compared to their respective binder analogues. The Tafel slopes were generally larger for the composites, with WC-FeCoNi being the exception.

To enable a direct comparison of corrosion rates between the binder analogues and the binders within the composites, the corrosion currents of the composites were normalized for the binder's surface area since only the metallic binder oxidizes at OCP. In general, the corrosion rates are higher in the composites, especially in WC-CoNi, WC-CoCr, WC-NiCr, WC-FeCoNi, and WC-CoNiCr. The order of corrosion rates in the binders was Co > FeCoNi > CoNi ≈ Ni > NiCrMo > CoCr > CoNiCr > NiCr, being close in the last 4 binders. A different order was found for composites: WC-FeCoNi > WC-Co > WC-CoCr > WC-CoNiCr ≈ WC-CoNi > WC-NiCr > WC-Ni > WC-NiCrMo. A direct comparison of binders and composites cannot be made at this moment since the binder analogues have a composition slightly different from the binders in the composites (Table 2). The corrosion rate order of the composites can be arranged in three groups: > 20 $\mu A\ cm^{-2}$ (WC-Co and WC-FeCoNi), 10–20 $\mu A\ cm^{-2}$ (composites with Co-based binders), and 1–3 $\mu A\ cm^{-2}$ (composites with Ni-based binders).

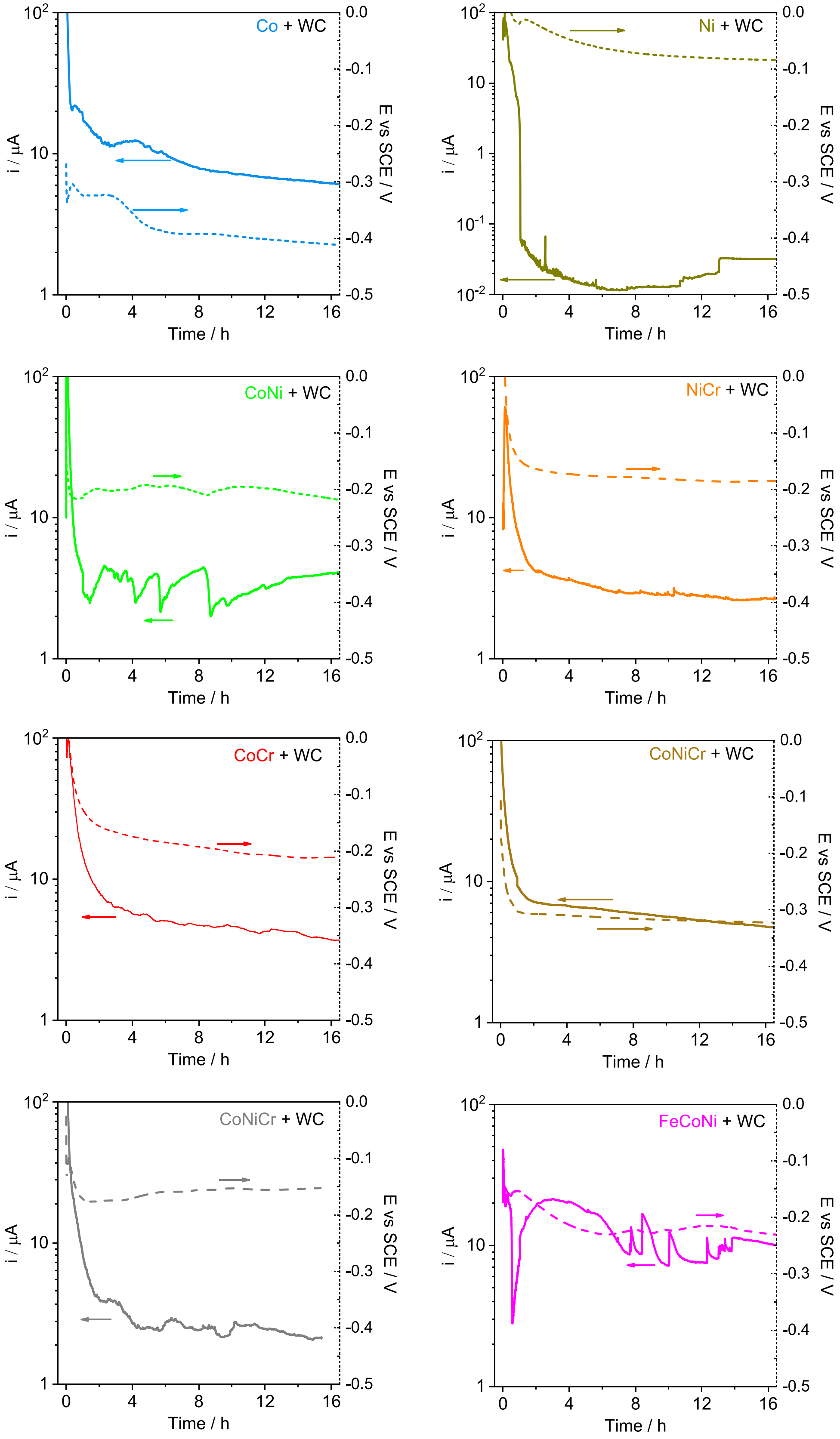

Fig. 8. Galvanic current and couple potential of WC with the various binders immersed in 0.5 M NaCl.

3.2.3. Reconstruction of current-potential curves

An attempt was made to reconstruct the polarisation curves of the composites using the individual curves of WC and binder analogues. Fig. 6 illustrates this attempt for WC-Co. In Fig. 6 a), the WC-Co curve is presented alongside the curves of Co and WC, both adjusted for the respective area fractions of each phase [22].

The intersection point of the anodic (Co) and cathodic (WC) curves is expected to correspond to the corrosion potential (E_{corr}) and corrosion current (i_{corr}) of the composite, denoted by a red dot in Fig. 6 a). These values, together with the experimental E_{corr} and i_{corr}, are given in Fig. 6 a). The reconstructed WC-Co curve presented in Fig. 6 b) deviates from the experimental WC-Co curve. This discrepancy becomes more pronounced above 0.4 V vs SCE, as the experimental current drop cannot be predicted from the partial polarisation curves of Co and WC. The current drop is attributed to processes that occur only when both phases are present in the composite: WC skeleton and protective oxides from the dissolved W in the binder. Consequently, the combination of partial curves to reconstruct the overall response is not valid in this case due to the complexity of the reactions taking place. The approach may still hold validity in the vicinity of the corrosion potential, depending on the reproducibility and validity of the input curves and curve used for comparison.

Regarding reproducibility, Fig. 7 displays repeated polarisation curves for Co, WC, and WC-Co, obtained with fresh new surfaces from 2 or 3 different sintered samples of each system. Despite the similarities, small variations exist that can impact the quality of the reconstruction and the comparison with the experimental curve. The estimates of E_{corr} and i_{corr} obtained from the intersection of the anodic and cathodic curves are presented in Table 5 for all composites. In general, the estimates closely align with the experimental values.

3.2.4. Galvanic coupling between WC and binder

In another experiment, the galvanic corrosion of the composites was simulated by galvanically coupling WC with the analogue binders. The exposed area of each electrode was delimited so that the sum of the areas was 1 cm^2 and their ratio obeyed the values in Table 1. Over a period of 16 h, the galvanic current (i_{Galv}) and couple potential (E_{couple}) were continuously measured. The results of this experiment are depicted in Fig. 8. Both i_{Galv} and E_{couple} decreased during the first 1–2 h stabilising in relatively constant values afterwards. Most of the current values were around 10 μA. The exception was Ni with a very low current in the order of 10 nA. The values of E_{couple} and i_{Galv} measured after 1 h and 16 h are presented in Table 5. In general the galvanic current is significantly higher than the corrosion rates of the composites. This suggests that the galvanic coupling is less effective in the composites. It appears that the reduction of oxygen is easier when the WC and the binder are not in close proximity.

However, such a conclusion must be postponed since the binder analogues used in the measurements do not exactly match the chemical composition of the binder within the hardmetal composites. The dissolved W can enhance the alloys resistance to oxidation [19,35], therefore it is likely to expect a decrease in the galvanic current with more corrosion resistance anodes. This experiment must, and will, be repeated with new binders analogues with the same composition as the binders in the composites. The importance of the dissolved W in the binder will be verified then.

4. Conclusions

In this study, the corrosion behaviour of various hardmetals was compared to that of binder analogues manufactured with compositions based on the composites starting raw materials. The corrosion potential of the hardmetals was more positive than that of the binders. The corrosion rates of the studied hardmetals were > 20 μA cm^{-2} for WC-Co and WC-FeCoNi, 10–20 μA cm^{-2} for composites with Co-based binders, and 1–3 μA cm^{-2} for composites with Ni-based binders. The corrosion rates of the binders in the composites were higher than the corrosion rates of the binder analogues. The attempt to reconstruct the polarisation curves of the composites using the individual curves of the binders and WC was not successful due to the complex response of the composites, which involved processes that only occur when both phases are present. However, estimating E_{corr} *and* i_{corr} from the intersection of the anodic (binder) and cathodic (WC) curves resulted in values that closely matched the experimental values. The galvanic currents between WC and the binders were significantly higher than the corrosion rates of the composites. A likely explanation for the discrepancies observed in the reconstruction of the polarisation curves and for the higher galvanic currents, is the mismatch of the composition of the binder analogues and the binders within the hardmetal composites. The later contain dissolved tungsten that enhances the resistance to oxidation. Experiments should be repeated with new binder analogues containing the right amount of tungsten. Then a better comparison can be made between composites and binders and the true impact of tungsten verified.

Author statement

The authors A.M. Ferro Rocha, A.M. Santos, R. Mineiro, P. Pereira, J. Sacramento, A.M.R. Senos, and A.C. Bastos, declare that the revised manuscript entitled “**Prediction of hardmetal corrosion based on the binder response**”, submitted to *International Journal of Refractory Metals and Hard Materials* is original and not being considered for publication elsewhere.

Declaration of Competing Interest

The authors declare no conflict of interest.

Data availability

Data will be made available on request.

Acknowledgements

This work was developed within the scope of the project CICECO-Aveiro Institute of Materials, UIDB/50011/2020, UIDP/50011/2020 & LA/P/0006/2020, financed by national funds through the FCT/MEC (PIDDAC), and project HARDTECH–POCI–01-0247-FEDER-045283, financed by FEDER under PT2020 Partnership Agreement.

A.M. Ferro Rocha thanks FCT for the PhD grant SFRH/BD/147060/2019. A.C. Bastos is funded by national funds (OE), through FCT - Fundação para a Ciência e a Tecnologia, I.P., in the scope of the framework contract foreseen in the numbers 4, 5 and 6 of the article 23, of the Decree-Law 57/2016, of August 29, changed by Law 57/2017, of July 19.

References

[1] G.S. Upadhyaya, Cemented Tungsten Carbides: Production, Properties and Testing, Noyes Publications, New Jersey (US), 1998.

[2] V.K. Sarin, D. Mari, L. Llanes, C.E. Nebel (Eds.), Comprehensive Hard Materials I–III, Elsevier, Oxford (UK), 2014.

[3] L. Prakash, Fundamentals and general applications of hardmetals, Comprehens. Hard Mater. 1 (2014) 29–90.

[4] Report on carcinogens background document for cobalt–tungsten carbide: powders and hard metals, in: National Toxicology Program, U.S. Department of Health and Human Services, 2009 available online, https://ntp.niehs.nih.gov/sites/default/files/ntp/roc/twelfth/2010/finalbds/hardmetals bd20100408_508.pdf (last retrieved on June 25, 2023).

[5] Report on carcinogens monograph on cobalt and cobalt compounds that release cobalt ions in vivo, in: National Toxicology Program, U.S. Department of Health and Human Services, 2016 available online, https://ntp.niehs.nih.gov/publications/roc/rocmgraph06. last retrieved on June 25, 2023.

[6] https://echa.europa.eu/substance-information/-/substanceinfo/100.028.325 (last retrieved on June 25, 2023).

[7] Critical Raw Materials Resilience: Charting a Path towards greater Security and Sustainability, available online, https://eur-lex.europa.eu/legal-content/EN/TXT/PDF/?uri=CELEX:52020DC0474, 2020 (last retrieve on June 25, 2023).

[8] S. Norgren, J. Garcia, A. Blomqvist, L. Yin, Trends in the P/M hard metal industry, Int. J. Refract. Met. Hard Mater. 48 (2015) 31–45.

[9] M. de Nicolás, H. Besharatloo, P. Alvaredo, J.J. Roa, L. Llanes, E. Gordo, Design of alternative binders for hard materials, Int. J. Refract. Met. Hard Mater. 87 (2020), 105089.

[10] P. Pereira, A.M.F. Rocha, J. Sacramento, F.J. Oliveira, A.M.R. Senos, L. F. Malheiros, A.C. Bastos, Corrosion resistance of WC hardmetals with different co and Ni-based binders, Int. J. Refract. Met. Hard Mater. 104 (2022), 105799.

[11] A.M. Ferro Rocha, A.C. Bastos, J.P. Cardoso, F. Rodrigues, C.M. Fernandes, E. Soares, J. Sacramento, A.M.R. Senos, M.G.S. Ferreira, Corrosion behaviour of WC hardmetals with nickel-based binders, Corros. Sci. 147 (2019) 384–393.

[12] A. Human, H. Exner, The relationship between electrochemical behaviour and inservice corrosion of WC based cemented carbides, Int. J. Refract. Met. Hard Mater. 15 (1997) 65–71.

[13] P.K. Katiyar, P.K. Singh, R. Singh, A.L. Kumar, Modes of failure of cemented tungsten carbide tool bits (WC/co): a study of wear parts, Int. J. Refract. Met. Hard Mater. 54 (2016) 27–38.

[14] R.J.K. Wood, S. Herd, M.R. Thakare, A critical review of the tribocorrosion of cemented and thermal sprayed tungsten carbide, Tribol. Int. 119 (2018) 491–509.

[15] G.D. Mohan, B.E. Klamecki, The susceptibility of wood-cutting tools to corrosive wear, Wear 74 (1981–1982) 85–92.

[16] W.J. Tomlinson, I.D. Molyneux, Corrosion, erosion-corrosion, and the flexural strength of WC-co hardmetals, J. Mater. Sci. 26 (1991) 1605–1608.

[17] A.M. Human, B. Roebuck, H.E. Exner, Electrochemical polarisation and corrosion behaviour of cobalt and Co(W,C) alloys in 1 N sulphuric acid, Mater. Sci. Eng. A 241 (1998) 202–210.

[18] V.A. Pugsley, G. Korn, S. Luyckx, H.-G. Sockel, W. Heinrich, M. Wolf, H. Feld, R. Schulte, The influence of a corrosive wood-cutting environment on the mechanical properties of hardmetal tools, Int. J. Refract. Met. Hard Mater. 19 (2001) 311–318.

[19] S. Sutthiruangwong, G. Mori, Corrosion properties of Co-based cemented carbides in acidic solutions, Int. J. Refract. Met. Hard Mater. 21 (2003) 135–145.

[20] S. Hochstrasser-Kurz, Y. Mueller, C. Latkoczy, S. Virtanen, P. Schmutz, Analytical characterization of the corrosion mechanisms of WC-co by electrochemical methods and inductively coupled plasma mass spectroscopy, Corros. Sci. 49 (2007) 2002–2020.

[21] P. Pereira, A.M. Ferro Rocha, J. Sacramento, F.J. Oliveira, L.F. Malheiros, A.M. R. Senos, A.C. Bastos, Effect of different acidic media on the corrosion behaviour of hardmetals with Ni-based binders, Int. J. Refract. Met. Hard Mater. 110 (2023), 106019.

[22] A.M. Human, H.E. Exner, Electrochemical behaviour of tungsten-carbide hardmetals, Mater. Sci. Eng. A 209 (1996) 180–191.

[23] L.H. Hihara, R.M. Latanision, Corrosion of metal matrix composites, Int. Mater. Rev. 39 (1994) 245–264.

[24] C. Wagner, W. Traud, Über die Deutung von Korrosionsvorgängen Durch Überlagerung von Elektrochemischen Teilvorgängen und Über die Potentialbildung an Mischelektroden, Zeitschrift Für Elektrochemie und Angewandte Physikalische Chemie 44 (1938) 391–402; English translation by F. Mansfeld: On the Interpretation of Corrosion Processes Through the Superposition of Electrochemical Partial Processes and on the Potential of Mixed Electrodes, Corrosion (NACE) 62, 2006, p. 844.

[25] D.A. Jones, Principles and Prevention of Corrosion, 2nd Ed, Prentice-Hall, 1996.

[26] P. Pereira, L.M. Vilhena, J. Sacramento, A.M.R. Senos, L.F. Malheiros, A. Ramalho, Abrasive wear resistance of WC-based composites, produced with co or Ni-rich binders, Wear 482-483 (2021), 203924.

[27] A.F. Rocha, A. Bastos, J. Cardoso, F. Rodrigues, C. Fernandes, E. Soares, J. Sacramento, A. Senos, M. Ferreira, Corrosion behaviour of WC hardmetals with nickel-based binders, Corros. Sci. 147 (2019) 384–393.

[28] W. Schubert, H. Neumeister, G. Kinger, B. Lux, Hardness to toughness relationship of fine-grained WC-co hardmetals, Int. J. Refract. Met. Hard Mater. 16 (1998) 133–142.

[29] J.D. Voorhies, Electrochemical and chemical corrosion of tungsten carbide (WC), J. Electrochem. Soc. 119 (1972) 219–222.

[30] M.C. Weidman, D.V. Esposito, I.J. Hsu, J.G. Chen, Electrochemical stability of tungsten and tungsten monocarbide (WC) over wide pH and potential ranges, J. Electrochem. Soc. 157 (2010) F179–F188.

[31] M. Pourbaix, Atlas of Electrochemical Equilibria in Aqueous Solutions, NACE, 1974.

[32] M. Itagaki, A. Matsuzaki, K. Watanabe, The electrochemical impedance response of transpassive dissolution of chromium in neutral solutions containing sodium chloride and sodium fluoride, Corros. Sci. 37 (1995) 1867–1878.

[33] W.J. Tomlinson, C.R. Linzell, Anodic polarization and corrosion of cemented carbides with cobalt and nickel binders, J. Mater. Sci. 23 (1988) 914–918.

[34] M. Anik, Effect of concentration gradient on the anodic behavior of tungsten, Corros. Sci. 48 (2006) 4158–4173.

[35] S. Sutthiruangwong, G. Mori, R. Kösters, Passivity and pseudopassivity of cemented carbides, Int. J. Refract. Met. Hard Mater. 23 (2005) 129–136.

[36] R. Steinlechner, R. de Oro Calderon, T. Koch, P. Linhardt, W.D. Schubert, A study on WC-Ni cemented carbides: constitution, alloy compositions and properties, including corrosion behaviour, Int. J. Refract. Met. Hard Mater. 103 (2022), 105750.

[37] R.F. Santos, A.M.F. Rocha, A.C. Bastos, J.P. Cardoso, F. Rodrigues, C.M. Fernandes, J. Sacramento, M.G.S. Ferreira, A.M.R. Senos, C. Fonseca, M.F. Vieira, L. F. Malheiros, The effect of Cr content on the corrosion resistance of WC-Ni-Cr-Mo composites, Int. J. Refract. Met. Hard Mater. 95 (2021), 105434.

[38] R.F. Santos, A.M.F. Rocha, A.C. Bastos, J.P. Cardoso, F. Rodrigues, C.M. Fernandes, J. Sacramento, M.G.S. Ferreira, A.M.R. Senos, C. Fonseca, M.F. Vieira, L. F. Malheiros, Microstructural characterization and corrosion resistance of WC-Ni-Cr-Mo composite - the effect of Mo, Int. J. Refract. Met. Hard Mater. 86 (2020), 105090.